JOURNAL OF BACTERIOLOGY, Nov. 1989, p. 6279–6287
0021-9193/89/116279-09$02.00/0

Vol. 171, No. 11

Multiple Kinetic States for the Flagellar Motor Switch

SCOT C. KUO† AND DANIEL E. KOSHLAND, JR.*

Department of Biochemistry, University of California, Berkeley, California 94720

Received 20 April 1989/Accepted 25 July 1989

By means of a computerized video processing system, the flagellar motors of *Escherichia coli* were shown to have multiple kinetic states for each rotational direction. High-resolution analysis of flagellar motors revealed new kinetic states both in wild-type cells and in a strain deleted of other signal-transducing genes to which CheY had been introduced. This strain, RP1091, retained residual kinase activity that could phosphorylate CheY, complicating the biochemical identification of certain kinetic states. The behavioral effect of CheY on single flagellar motors was ultrasensitive, with an apparent Hill coefficient of 5.5 ± 1.9 (SD) and a half-maximal effect at 10.1 ± 0.5 (SD) μM CheY. Based on the CheY concentration dependence, a two-state model is clearly excluded, even for the simpler system of CheY-induced rotational reversals in the deletion strain. The data are best described by a four-state model, with two clockwise and two counterclockwise states.

The ability to follow the switching behavior of single biomolecules can provide great insights into molecular events of switching. Biological switches abound in nature, but only a few can be analyzed as single entities. Gated ion channels, some of which are critical to the generation and propagation of neuronal action potentials, are well-studied examples. Techniques such as black-lipid reconstitution (2), patch-clamp measurements (1, 42), and single-channel recording (30) have provided insights which, prior to these techniques, could only be indirectly inferred from the behavior of a large population of molecules.

Another biological switch amenable to analysis as a single complex is the rotational switch controlling the bacterial flagellar motor. Peritrichous bacteria, such as *Escherichia coli*, swim by the action of several passive helical filaments driven by rotary motors coupled to proton motive force (23). The behavior of single flagellar motors can be examined by tethering uniflagellate bacteria (25, 37). Tethered by anti-flagellin antibodies, cell bodies rotate when torque is applied to the immobilized flagellar filament. Motors rotate at constant angular velocity in either rotational direction, and rotational reversals occur abruptly (3). When cells respond to attractants, they transiently suppress tumbling, and the motors rotate exclusively counterclockwise during the response, resulting in smooth swimming (3, 8, 24). Changes in proton motive force can also alter the steady-state switching probabilities between rotational directions (17).

Based on the binary nature of bacterial swimming and the isolation of certain bacterial mutants, it has been proposed that a switch regulates motor behavior (18, 33, 34, 36, 47, 48). Chemotaxis mutants, which show aberrant accumulation in chemical gradients, have been used to identify components of this switch. Mutations in the switch genes can be complemented by mutations in other switch components (47) or by mutations in two chemotaxis genes, *cheY* and *cheZ* (33, 34, 47).

These two chemotaxis genes, *cheY* and *cheZ*, express proteins that play crucial roles in controlling the switch for flagellar rotational direction. CheY makes motors rotate clockwise, both in vivo, using inducible promoters for CheY expression (10, 20, 45), and in vitro, where CheY is reconstituted into bacterial spheroplasts (35). CheZ counteracts the effect of CheY in free-swimming cells (20). Recently, CheY has been phosphorylated in vitro (14–16, 46), probably enhancing its ability to induce clockwise rotation (39).

In view of the importance of motor switching in understanding chemotaxis and its value as another example of a molecular switch, the detailed kinetics of motor switching was examined.

MATERIALS AND METHODS

Materials. 5-Bromo-4-chloro-3-indolyl-β-D-galactopyranoside (X-gal), isopropyl-β-D-thiogalactopyranoside (IPTG), and 5-bromo-4-chloro-3-indolyl phosphate (BCIP) were from Sigma Chemical Co. (St. Louis, Mo.). Restriction endonucleases, calf intestinal alkaline phosphatase, T4 DNA ligase, and alkaline phosphatase-conjugated goat anti-rabbit antibodies were purchased from Boehringer Mannheim Biochemicals (Indianapolis, Ind.).

^{125}I-protein A was purchased from ICN Radiochemicals (Irvine, Calif.), and [γ-^{32}P]ATP was purchased from Amersham Corp. (Arlington Heights, Ill.). Nitrocellulose (BA85; 0.45-μm pores) and DEAE-nitrocellulose (NA45) were purchased from Schleicher & Schuell, Inc. (Keene, N.H.). Rabbit polyclonal anti-CheA (α-CheA), α-CheY, and α-CheZ antibodies were kindly provided by A. M. Stock (40, 41).

Strains. All strains used in this study are derived from *E. coli* K-12 and are listed in Table 1.

Cloning and strain constructions. DNA manipulations were performed as described by Maniatis et al. (28). Restriction enzymes and DEAE-nitrocellulose were used as recommended by the supplier. As shown in Fig. 1, single-copy versions of inducible expression of *cheY* were constructed from plasmid pCK62 (10) by a variation of the system described by Simons et al. (38) for examining single-copy promoters in *E. coli*. The host, D1210, was used to construct pKK80, and BMH7188 was used as the host for homologous recombination.

Lysogenic strains were constructed from RP1091 (32) by infecting liquid cultures with λKK41 phage at a multiplicity of infection of 5. Putative lysogens were genetically screened for resistance to λ *c*I90, sensitivity to λ *vir*, and growth on lactose as the sole carbon source (host strain carried *lacY*). Lysogens were also screened for motility and inducible CheY protein expression. Although certain isolates ap-

* Corresponding author.

† Present address: Department of Cell Biology and Physiology, Washington University Medical School, St. Louis, MO 63110.

TABLE 1. Bacterial strains

Strain	Relevant genotype	Parent	Source
BMH7118	F′ (*lacI*^{q} *lacZΔM15 proAB*) Δ(*lac-pro*) *thi-1*		P. Blum
D1210	*lacI*^{q}	HB101	R. Hallwell
DEK1080	λKK41 (*tac cheY lacZYA*)	RP1091	This study
RP437	F$^-$ *thr-1 leuB6 his-4 metF159 eda-50 rpsL136 thi-1 ara-14 mtl-1 xyl-5 tonA31 tsx-78*		J. S. Parkinson
RP1091	Δ(*cheA-cheZ*)*2209 eda*$^+$	RP437	32

peared to have multicopy lysogens, the isolate with the least amount of CheY expression was used for behavioral studies and was designated DEK1080.

Protein purification. The CheY substrate was purified by the method of Stock et al. (40). CheA and CheA-CheZ (A/Z) fusion proteins were partially purified by the following procedure. Three liters (7 g of cells) each of RP1091 and RP437 were grown aerobically at 30°C in Vogel-Bonner medium E (44), supplemented with 1% (wt/vol) glycerol, thiamine (20 μg/ml), and 200 μg each of histidine, methionine, leucine, and threonine (VBC-HMLTT) per ml to mid-log phase (OD_{650}, ≈1.2), and washed with TE (10 mM Tris hydrochloride [Tris(HCl)], 1 mM EDTA, pH 7.5). Cells were lysed in TE with a French pressure cell and clarified by centrifugation at 14,500 × *g* for 15 min, followed by high-speed centrifugation at 110,000 × *g* for 1 h. The supernatant was precipitated at 0°C with 30% ammonium sulfate and dialyzed against 10 mM Tris(HCl), pH 7.4, buffer at 5°C. With a MonoQ HR 5/5 anion-exchange fast protein liquid chromatography column from Pharmacia and a linear gradient of 0 to 1 M NaCl in 10 mM Tris(HCl), pH 7.4, at 5°C, the peaks of CheA and A/Z proteins eluted between 350 and 430 mM NaCl and were pooled. Subsequent purification was performed in a linear gradient of 10 to 300 mM $NaPO_4$, pH 7.2, at 5°C on a hydroxyapatite column from Mitsui Toatsu Chemical, Inc. (Tokyo). Peak CheA and A/Z proteins eluted between 135 and 170 mM $NaPO_4$ and were concentrated by a 100-μl DE52 anion-exchange minicolumn poured in a 200-μl pipette tip [stepwise elution with 0 to 500 mM NaCl in 10 mM Tris(HCl), pH 7.4]. Protein purification was monitored by immunoblot analysis (46) as modified by Kuo and Koshland (20) with α-CheA and α-CheZ antibodies. By this procedure, CheA from RP437 had detectable CheZ contamination. All labeling reactions were performed in 100 μM ATP (3 Ci of [γ-^{32}P]ATP per mmol)–50 mM KCl–0.2 mM EDTA–0.5 mM $MgCl_2$–2.4 mM dithiothreitol–20% (wt/vol) glycerol–50 mM Tris(HCl), pH 8.6. For time points, reactions were stopped by the addition of sodium dodecyl sulfate sample buffer and immediate freezing in liquid nitrogen.

Protein quantitation. CheY expression levels were determined by a modification of immunoblot procedures (43) described previously (20). In sequential reactions, immunoreactive CheY was labeled with anti-CheY antibodies, ^{125}I-protein A, alkaline phosphatase-conjugated goat anti-rabbit antibodies, and again with ^{125}I-protein A. The alkaline phosphatase, visualized with BCIP by the method of Blake et al. (7), facilitated excision of CheY bands from the nitrocellulose for scintillation counting of the ^{125}I label. Larger samples in immunoblots further improved sensitivity. The detection limit of this assay is 10 ng of CheY per sample in cell extracts, equivalent to cytoplasmic concentrations of 4.7 μM CheY.

Tethering and tethering analysis. For all behavioral analyses, cells were grown aerobically at 30°C in VBC-HMLTT. The *tac* promoter was induced by harvesting and then resuspending cells in fresh VBC-HMLTT growth medium containing IPTG to grow aerobically at 30°C for 1 h. After excess flagella were sheared, cells were tethered by anti-flagellin antibodies as generally described by Macnab (25), and chloramphenicol (50 μg/ml) was used to inhibit further protein synthesis. The tethering chamber was constructed from stainless steel, as described by Berg and Block (4). Under dark-field illumination with a 200-W mercury arc lamp filtered by a Hoya 054 cutoff filter to remove blue light (27), tethered cells were videotaped with an RCA charge-coupled detector array camera, model TC2811, and a Panasonic AG-6300 videocassette recorder. The outlines of high-contrast videotape images were digitized with a Motion Analysis

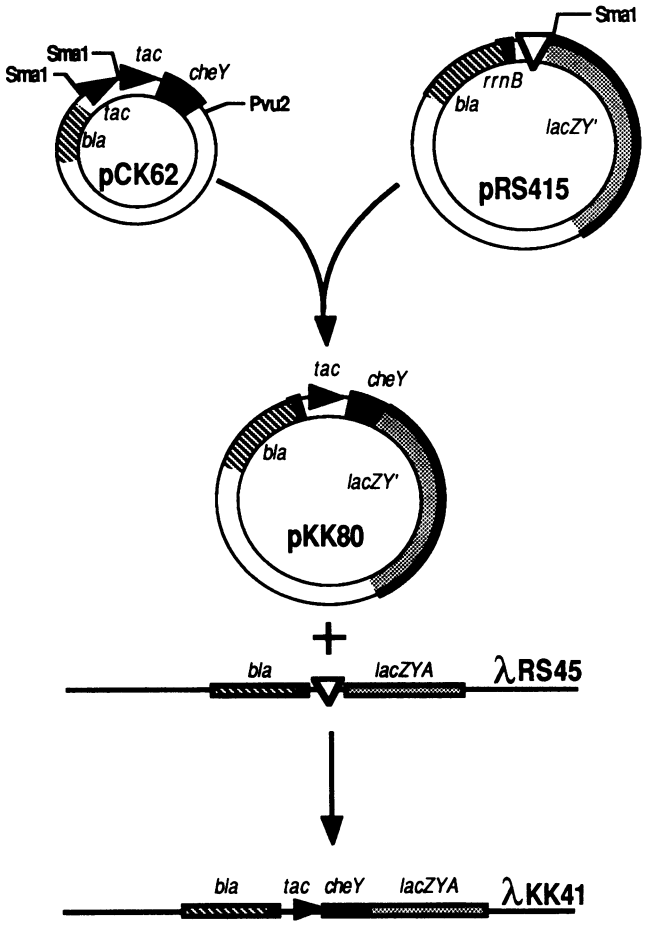

FIG. 1. Cloning strategy for inducible expression from single-copy *cheY* genes. Plasmid pCK62 (10), which contains the *tac* promoter controlling *cheY* expression, was digested with *Sma*I and *Pvu*II, and the 1.3-kilobase *tac-cheY*-containing DNA fragment was gel-purified with DEAE-nitrocellulose. The vector, pRS415 (38), was digested with *Sma*I and treated with alkaline phosphatase (to reduce the frequency of reclosed vector) prior to ligation with the purified *tac-cheY* fragment. Plasmid-bearing colonies were screened by β-galactosidase activity on the chromogenic substrate X-gal (20 μg/ml) and by inducible overproduction of CheY protein. Plasmid-bearing cells were superinfected with λRS45 (38), and subsequent λ phage lysates were screened with X-gal for recombinant phage.

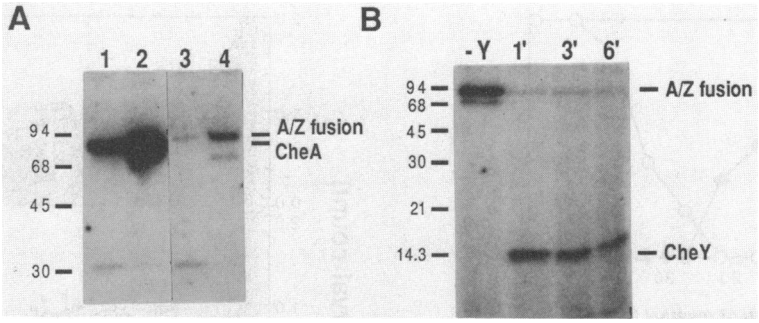

FIG. 2. Phosphorylation reactions of CheA and A/Z fusion protein from Δ(*cheA-cheZ*)*2209*. (A) CheA and A/Z fusion proteins from different purification steps were incubated with 100 μM [γ-^{32}P]ATP for 5 min at room temperature to assay for autophosphorylation activity. Each lane contains 1.8 μg of total protein. Molecular mass markers are indicated to the left (in kilodaltons). Lanes: 1, CheA from wild-type cells, MonoQ fraction; 2, CheA from wild-type cells, hydroxyapatite fraction; 3, A/Z fusion protein, MonoQ fraction; 4, A/Z fusion protein, hydroxyapatite fraction. The level of A/Z protein phosphorylation in lane 4 is 1/20 the level for CheA in lane 2. (B) Hydroxyapatite-purified A/Z fusion protein (0.3 mg of total protein) was incubated with 100 μM ATP for 10 min at room temperature prior to 0°C incubation with (lane 1) TE buffer, 6 min; (lane 2) 1 μg of CheY protein, 1 min; (lane 3) 1 μg of CheY protein, 3 min; (lane 4) 1 μg of CheY protein, 6 min. Phosphotransferase reactions were performed on ice to enhance the steady-state levels of phosphorylated CheY.

VP-110 (Santa Rosa, Calif.) at a 60-Hz sampling rate. Lacking appropriate software, we developed our own analysis programs in Microsoft C supplemented by HALO graphics subroutines (Media Cybernetics, Inc.) on an IBM PC/AT.

All dwell-time histograms were constructed by using uniformly sized bins. Fits to dwell-time histograms were done in one of two ways. If the histogram appeared to have multiple components, as judged by the semilogarithmic plots, nonlinear least-squares curve fitting was performed with a sum of exponentials by using the statistical package RS/1 (BBN Software Products Corp.) on an IBM PC/AT computer. If the histogram appeared to have only one component, the lifetime of the single exponential was estimated by using maximum-likelihood fits (11), assuming an instrument dead-time of 35 ms (see Fig. 3).

Cells to be examined by dwell-time analysis were screened by the following criteria. First, the cells had to be rotating energetically, usually at 3 to 10 Hz. Cells which stopped for long periods of time, presumably due to low proton motive force, were discarded from further analysis. Second, the cells had to switch rotational directions with temporally stable probabilities. This is easily screened by following the percent time spent rotating counterclockwise (%CCW) (in 15-s windows) as a function of tethering time. Cells showing a consistent drift in %CCW with time were discarded from further analysis.

RESULTS

Single-copy construction for CheY expression. To probe the molecular aspects of motor switching, we varied the cytoplasmic concentrations of CheY. In previous studies, we used heterologous, inducible promoters to control the expression of CheY (10, 20). To decrease the uninduced expression levels, we reduced the gene dosage by the strategy shown in Fig. 1 by using lysogenized λ phage as an expression vector (38). For the experiments reported here, we used the host strain RP1091 (32), which contains the genomic deletion Δ(*cheA-cheZ*)*2209*. The deletion extends through all the cytoplasmic chemotaxis components as well as some of the integral membrane receptors for chemotaxis. Without induction, the CheY concentration in the lysogenic construction was 5 μM (see Fig. 5), whereas wild-type cells have 8 μM CheY (20).

In addition to reducing CheY expression, single-copy constructions have another advantage over multicopy plasmids. The loss or gain of a single lysogenic copy has a large behavioral effect when the copy number is low. In particular, when RP1091 loses the λ lysogen expressing CheY, the cells rotate exclusively in the counterclockwise direction. This feature can be exploited to avoid analyzing cells that have lost the λ lysogen, reducing the amount of unnecessary analysis.

Residual kinase activities from Δ(*cheA-cheZ*)*2209* fusion protein. Recent studies (14–16, 46) have reconstituted the phosphotransferase reaction from CheA to CheY. Since the Δ(*cheA-cheZ*)*2209* deletion in RP1091 (32) generates a fusion protein (20), there was the possibility that the A/Z fusion protein retains kinase activity. This deletion has been the basis for numerous studies of "gutted" strains that lack any chemotaxis functions (10, 20, 39, 45). Although Δ(*cheA-cheZ*)*2209* has not been sequenced, deletion mapping indicates that the A/Z fusion protein retains approximately seven-eighths of CheA (32) and is larger than wild-type CheA because of additional CheZ sequences (20). By using a modified CheA purification procedure and α-CheA and α-CheZ immunoblots to monitor purification, we partially purified the A/Z fusion protein from RP1091. For comparison, a parallel purification of CheA was performed on the isogenic wild type, RP437. Comparable levels of CheA and A/Z fusion protein were expressed in the two strains.

The phosphorylation activities of the fusion protein are summarized in Fig. 2. The A/Z fusion protein could autophosphorylate itself (Fig. 2A). Autophosphorylation activity increased as the fusion protein was further purified, but the A/Z fusion protein autophosphorylated to only 1/20 the level of wild-type CheA. The A/Z fusion protein could also phosphorylate purified CheY, as shown in Fig. 2B. Thus, the A/Z fusion retained significant amounts of CheA activity, albeit less than the wild type.

Instrumentation for tethering analysis. Previously, videotapes of tethered bacteria were analyzed either manually (9, 21) or optically with linearly graded neutral-density filters (19). Berg et al. (5) recently described a custom electronic device to digitize video images for tethering analysis. However, we used a commercially available digitization instrument, manufactured by Motion Analysis, Inc., to process video images at a 60-Hz video sampling rate. Although the Motion Analysis instrument includes software to analyze translational motion of high-contrast objects, such as free-swimming bacteria, its software was poorly suited for the

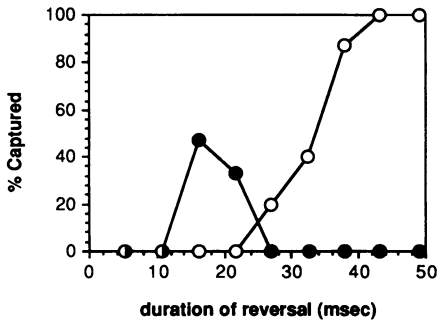

FIG. 3. Animated simulations to determine instrument resolution. Computer-generated, high-resolution graphic images were used to simulate the dark-field images of rotating bacteria. Animated images were generated at 15.4 Hz and videotaped at 60 Hz, and analysis was performed at a 5-Hz sampling rate of the videotape. On average, each animation image had an effective duration of 5.4 ms in the analysis and an angular velocity of 9.2 Hz. Effectively, clockwise intervals were maintained at 76 ms, and counterclockwise intervals were at various multiples of 5.4 ms. The instrument's efficiency of detecting 15 counterclockwise intervals is plotted against the duration of those counterclockwise intervals. Open circles show the frequency with which counterclockwise intervals were properly identified as counterclockwise intervals; solid circles show the frequency with which counterclockwise intervals were mistakenly identified as stops or pauses.

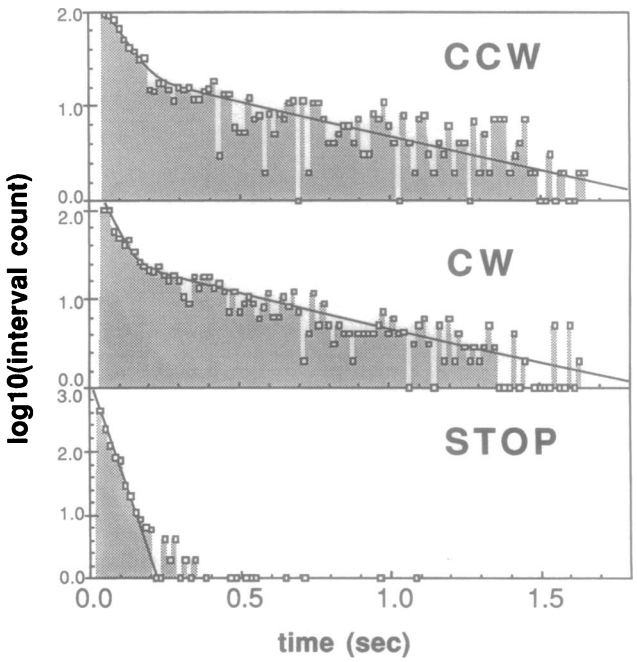

FIG. 4. Dwell-time histograms for wild-type cells. Wild-type cells (RP437) were tethered, and a single cell was videotaped for 24 min and analyzed as described in Materials and Methods. Histogram points show the number of rotational events (log scale) that persisted for the 17-ms time segments (bins). Shading emphasizes that this is a histogram. Larger bins would have smoothed the curve but preserved the area under the curve. There were 1,263, 1,085, and 1,072 events to construct the CCW, CW, and Stop histograms, respectively. Results from nonlinear least-squares fitting to these histograms are listed in Table 2.

analysis of rotating bacteria. Therefore, we developed a software package (manuscript describing this software is in preparation) for the purposes of this paper.

For practical reasons, the software defines three functional states for the flagellar motor. Two of these states are associated with active rotation of the motor, either clockwise or counterclockwise. The third state is an inactive motor which has stopped rotating. The stopped state, which can be of any duration, is observed more often with poorly energized bacteria.

To test the limitations of video analysis, we developed a graphics computer program to display a simulation of rotating bacterial images. This program can generate images at 60 Hz, which were videotaped and subsequently analyzed. Videotapes were analyzed at a slower sampling rate, thereby increasing the effective speed and resolution of the animation sequence. As shown in Fig. 3, there was poor detection of intervals of less than 35 ms duration, which is approximately the duration of two video frames at the 60-Hz sampling rate. In fact, some of the shorter intervals were not just missed, but erroneously detected as short stops or pauses. For the purposes of this paper, the detection threshold was 35 ms.

Motor switching in wild-type cells. Using the new instrumentation and software, we reexamined the steady-state motor behavior of wild-type *E. coli*. Previous studies indicate that the flagellar motor switches rotational direction stochastically (6). From manual analysis of slow-playback videotapes, histograms of motor dwell-times were well approximated by single exponential functions (9). Although their resolution was 150 ms, their detection threshold was estimated at 400 ms, leading them to conclude that a two-state model (9), similar to equation 1 below, was sufficient.

Figure 4 shows the dwell-time histograms derived from automated analysis of a wild-type bacterial cell. The histograms are presented on a semilogarithmic scale to make exponential components more apparent. Clearly, the histograms, both for clockwise and for counterclockwise intervals, were not single exponentials. Short rotational intervals, less than 250 ms in duration, were more frequent than predicted by a single-exponential distribution. For both clockwise and counterclockwise histograms, a sum of two exponential functions was a better description, and the results from nonlinear least-squares fitting to the dwell-time histograms are listed in Table 2.

CheY-induced motor switching. Using the single-copy *tac-cheY*-inducible expression system, we altered the behavior of the Δ(*cheA-cheZ*) deletion strain, which lacks the cytoplasmic chemotaxis components. Figure 5 shows the effect of CheY on the percent time spent rotating clockwise (%CW). The behavioral effect of CheY expression has a half-maximal effect at cytoplasmic concentrations of 10.1 ±

TABLE 2. Nonlinear least-squares analysis of wild-type dwell-time histograms[a]: $y = n_1\exp(-\lambda_1 t) + n_2\exp(-\lambda_2 t)$

Interval type	n_1	λ_1 (s^{-1})	n_2	λ_2 (s^{-1})
CCW	0.907 (±4%)	12.6 (±7%)	0.093 (±17%)	1.0 (±20%)
CW	0.862 (±6%)	19.0 (±8%)	0.138 (±11%)	1.8 (±10%)
Stop	1.000 (±3%)	33.8 (±2%)	—[b]	—

[a] Normalization factors were used so that the histogram distributions became probability distribution functions (p.d.f.) where $y = 1$ at time $t = 0$ and n_1 and n_2 are dimensionless weighting factors. These factors are: CCW, 151; CW, 180; and Stop, 1,316. Error estimations are standard deviations of nonlinear least-squares curve fitting.

[b] —, Stop intervals were fit to a single exponential function as the p.d.f. (n_2 is zero).

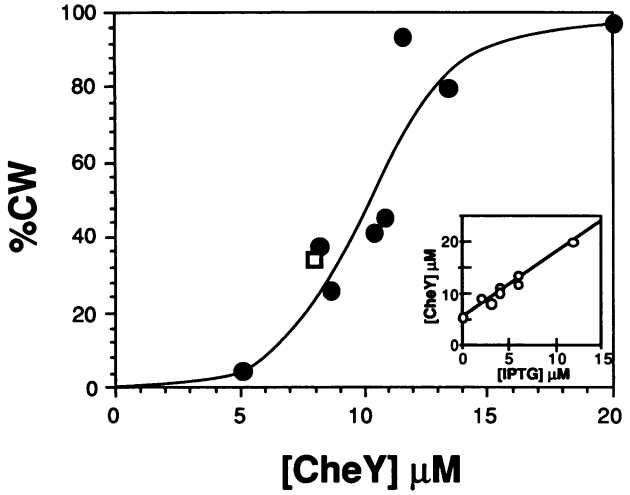

FIG. 5. Dose dependence of CheY-induced clockwise rotation. Cells of strain DEK1080, which is RP1091 [Δ(*cheA-cheZ*)] lysogenized with λKK41 carrying *tac-cheY*, were induced with IPTG and tethered with antiflagellin antibodies. %CW was calculated as the percent total rotating time (Stops excluded from calculation) that cells rotated clockwise. For cells of the same culture, average %CW is reported. The sigmoidal curve was generated by using the Hill equation. Nonlinear least-squares fitting, using the RS/1 statistical analysis package, estimated a Hill coefficient of 5.5 ± 1.9 and a half-maximal effect at 10.1 ± 0.5 μM CheY (errors are standard deviations). The open square point is from the wild-type bacterium RP437 in Fig. 4. (Inset) Apparent linearity of CheY induction from the single-copy *tac-cheY* with low amounts of IPTG.

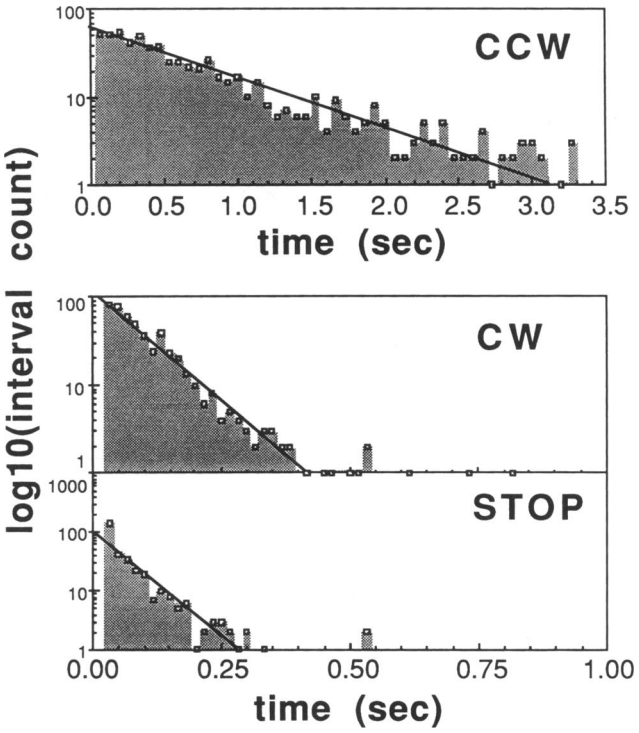

FIG. 7. Dwell-time histograms for CheY-induced reversals in a Δ(*cheA-cheZ*) strain. This cell is from the same culture used in Fig. 6, which has cytoplasmic CheY concentrations of 10.3 μM. Bins in the histogram were either 67 ms for CCW distribution or 17 ms for CW and Stop distributions. From 31.5 min of videotape information, there were 733, 488, and 320 events for the CCW, CW, and Stop distributions, respectively. Assuming single-exponential distributions, maximum-likelihood estimates show the rate constants to be 0.65, 8.1, and 13 s^{-1} for the CCW, CW, and Stop distributions, respectively.

0.5 (SD) μM CheY. The shape of the behavioral response curve was sigmoidal, with an apparent Hill coefficient of 5.5 ± 1.9 (SD). Figure 6 shows that changes in rotational direction happened suddenly (usually <50 ms), and the magnitude of angular velocities was the same in either rotational direction. Qualitatively, CheY-induced reversals were similar to wild-type reversals (3).

Figure 7 shows a sample dwell-time histogram for CheY-induced reversals in the Δ(*cheA-cheZ*) deletion strain. Determined by a parallel culture, the IPTG-induced expression in this cell of CheY was 10.3 μM in the cytoplasm. On the semilogarithmic plots, only one exponential component was apparent for both the clockwise and counterclockwise distributions. By using maximum-likelihood estimates that assume a single-exponential distribution, the rate constants of counterclockwise and clockwise distributions were 0.65 and 8.1 s^{-1}, respectively.

The lack of extra exponential components to the dwell-time distribution in the Δ(*cheA-cheZ*) deletion strain does not contradict results from wild-type cells. In wild-type cells, the extra chemotaxis components, which are missing in the Δ(*cheA-cheZ*) mutant, might be responsible for the extra kinetic states. With only CheY present, the flagellar motor might show simpler switching kinetics. The simplest kinetic model for CheY-induced reversals in Δ(*cheA-cheZ*) deletion mutants is based on a two-state model (9, 18, 33) and is expressed as

$$M_{ccw} \underset{k_{-1}}{\overset{k_1 Y}{\rightleftharpoons}} M_{cw} Y \qquad (1)$$

where M is the motor/switch complex, k_1 is the second-order

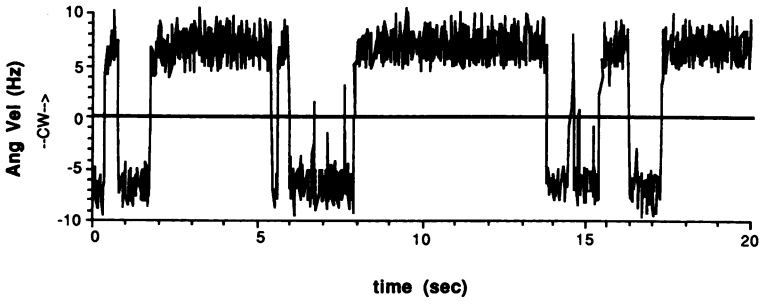

FIG. 6. Motor velocities for CheY-induced reversals in Δ(*cheA-cheZ*). Cells were prepared as described in the legend to Fig. 5. For this cell, the cytoplasmic concentration of CheY was estimated to be 10.3 μM. Ang Vel, Angular velocity.

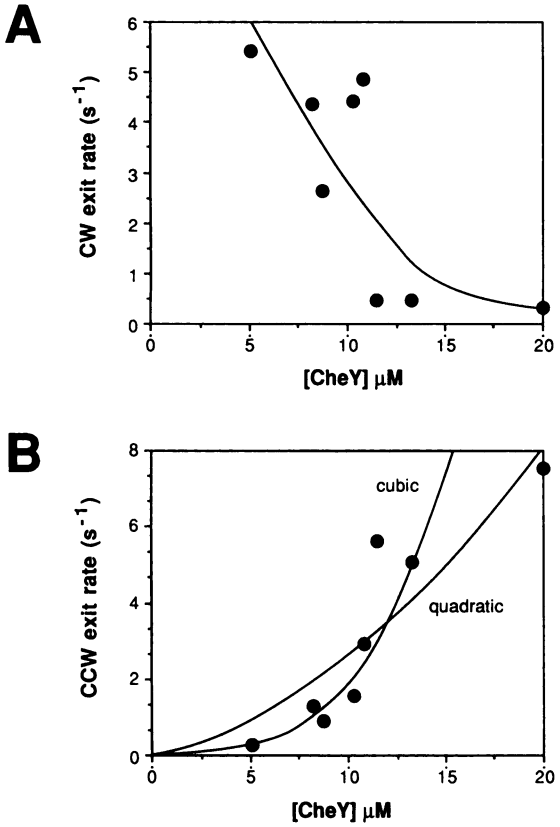

FIG. 8. Dose dependence of exit rates in CheY-induced reversals in a Δ(*cheA-cheZ*) strain. Cells were the same as those in Fig. 5. Exit rates were determined from dwell-time histograms by using maximum-likelihood estimates that assumed a single-exponential distribution. For cells in the same culture, the average exit rate is shown. (A) Clockwise exit rate. (B) Counterclockwise exit rate. Quadratic and cubic polynomial fits are also shown for the counterclockwise exit rates.

rate constant for generating clockwise rotation, k_{-1} is the first-order rate constant for ending clockwise events, and Y is the cytoplasmic concentration of active CheY. CheY is necessary for motors to reverse, and only two kinetic states are postulated, one for each rotational direction. From the data in Fig. 7, explicit values for k_1 and k_{-1} could be assigned for the two-state model (eqn. 1).

The two-state model, however, is not appropriate because it makes a strong prediction about the CheY concentration dependence for the duration of clockwise intervals. Although CheY is necessary for clockwise rotation, the duration of the clockwise intervals should be independent of CheY concentration, since it is determined by the first-order exit rate k_{-1}. Increasing CheY concentration would only affect the frequency of clockwise events, not their duration. The data in Fig. 8A clearly show that the clockwise exit rate decreased with CheY concentration, excluding the two-state model for CheY-induced reversals. CheY must affect at least two kinetically distinct clockwise states.

The duration of counterclockwise events also changed with the CheY concentration, but this feature is required of any CheY-dependent model. Models which assume only a single kinetic state for the counterclockwise rotational direction, such as the two-state model, predict a linear dependence of counterclockwise exit rates with the effective CheY concentration. A linear fit through the origin to the counterclockwise exit rates in Fig. 8B was not possible, but a quadratic or a cubic (third-order) polynomial fit through the origin is possible. A quadratic fit, however, was poorer than a cubic fit. These higher-order concentration dependencies suggest multiple steps in CheY-induced production of clockwise rotation from the counterclockwise state.

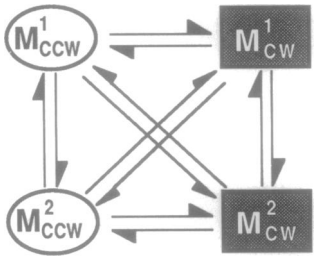

FIG. 9. Four-state kinetic model for motor reversals. M_{ccw} represents kinetic states where the flagellar motor rotates counterclockwise, and M_{cw} represents kinetic states where the motor rotates clockwise. Superscripts designate different kinetic states for the same rotational direction of the motor. For further clarity, counterclockwise states are enclosed in ovals, and clockwise states are enclosed in shaded rectangles.

DISCUSSION

Multiple states of the switch. Examining the bacterial flagellar motor with a computerized video processing system, we have shown that these rotary motors have multiple kinetic states for each rotational direction. The switching kinetics in wild-type cells reveal extra exponential components in the dwell-time distributions for flagellar motors in each rotational direction. These data exclude the two-state kinetic model proposed previously (9, 17, 33), and favor at least a four-state model, as shown in Fig. 9.

To distinguish among the more complicated models, we examined the subset of motor states induced by CheY in the Δ(*cheA-cheZ*) mutant background. In the absence of CheY, motors in this strain did not rotate clockwise, indicating that the rate of spontaneous reversals is less than 0.05 s^{-1}. The overall effect of CheY on single motors is to favor clockwise rotation, with a response that is sigmoidal. The apparent Hill coefficient is 5.5 ± 1.9, with a half-maximal effect at 10.1 ± 0.5 μM CheY. Although the dwell-time analysis of CheY-induced reversals showed only single-exponential distributions, the concentration dependence of these reversal rates indicates multiple kinetic states. Regardless of the mechanism of CheY activation, a two-state model (eqn. 1) is clearly excluded since it predicts that the duration of clockwise events is independent of CheY concentration. The data in Fig. 8A indicate that CheY must induce at least two clockwise kinetic states.

The two counterclockwise states observed in wild-type cells may also be due to multiple counterclockwise states induced by CheY. The CheY concentration dependence for the duration of counterclockwise intervals indicates multiple steps in producing clockwise rotation in the Δ(*cheA-cheZ*) mutant background. All these steps are not necessarily kinetic states of the motor, but some may reflect biochemical activation of CheY. The cubic (third-order) fit of Fig. 8B suggests three steps in producing clockwise rotation. If the biochemical activation of CheY has a first-order dependence on CheY concentration (most likely because CheY is a monomer), the remaining two steps must be kinetic states of the motor. A four-state model (Fig. 9), with two clockwise

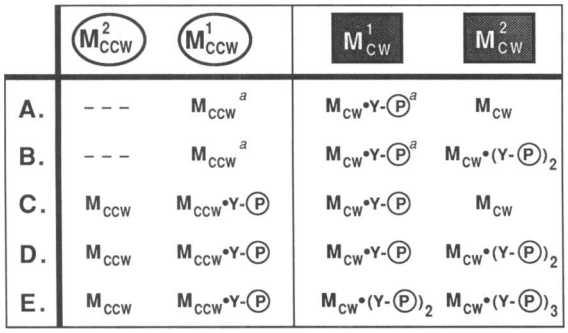

FIG. 10. Models for CheY-induced reversals in a Δ(*cheA-cheZ*) strain. Notations for motor states are as described in the legend to Fig. 9. The models with one counterclockwise state (marked with a superscript *a*) require that the steady-state generation of phosphorylated CheY have a second-order dependence on CheY concentration. The notation Y-P explicitly shows that phosphorylated CheY is the active species in affecting motor behavior (see text).

and two counterclockwise states, is the best explanation of all the kinetic data from both wild-type cells and CheY-induced RP1091 cells.

Presence of residual kinase activity. The discovery of residual kinase activity in the Δ(*cheA-cheZ*)*2209* deletion strain RP1091 has ramifications for the numerous studies of this deletion. In previous studies, it has been generally assumed that no CheA or CheZ functions remain in this deletion, since the deletion mutant does not complement either *cheA* or *cheZ* mutants. However, the existence of residual kinase activity leaves unresolved the question of whether unphosphorylated CheY can be effective in inducing clockwise rotation (10, 20, 39, 45). It also provides an alternative explanation for the effect of arsenate poisoning on CheY-induced reversals in this strain (39). Although a better *cheA-cheZ* deletion could be constructed to address these issues, crosstalk between the Ntr and Che phosphorylation systems would produce some phosphorylated CheY (31). Since the presence of phosphorylated CheY cannot be eliminated, it complicates the assignment of particular biochemical species to particular kinetic states. In the lack of contradictory evidence, our models will only consider phosphorylated CheY as the active species. If unphosphorylated CheY is also active, more kinetic states would be introduced into the models, increasing their complexity.

Molecular models. The discrete nature and limited resolution of video analysis can mistake rapidly reversing cells for frequently pausing cells. We found no evidence for the frequent, longer-lived pausing observed by Lapidus et al. (21) in wild-type cells. Although there is a selection bias for well-behaved cells, the pausing we observed is much more frequent and shorter-lived. Most of the pauses in wild-type cells were shorter than the 35-ms detection limit and cannot be characterized as genuine pauses (Fig. 3). Therefore, none of our models incorporate a paused state of the motor as a distinct kinetic state.

Addressing the natures of the multiple kinetic states observed in wild-type cells, the results from kinetic studies of CheY-induced reversals in RP1091 are summarized in the models presented in Fig. 10. In all the models, there are two clockwise states which differ by the association or dissociation of a single CheY monomer. As discussed previously, the possibility that there are less than two clockwise states was excluded by the data in Fig. 8A. Since a second-order dependence for CheY phosphorylation seems unlikely, we favor the models that include two counterclockwise states. Models 10A and 10B, which include only one counterclockwise state, are shown for completeness. All the models concentrate on the longer-lived states detectable by video microscopy. More complicated models are clearly possible, but are not necessary.

In all our studies of CheY-induced reversals in the Δ(*cheA-cheZ*) deletion strain, we have never seen the fast exponential component of the counterclockwise dwell-time distribution that is observed in wild-type cells. Clearly, some other processes, perhaps involving the wild-type CheA, are responsible for generating the shorter-lived counterclockwise intervals and the longer-lived clockwise intervals of wild-type cells.

Cooperativity and zero-order ultrasensitivity. The high sensitivity for the behavioral effect of CheY protein is particularly intriguing. Two types of molecular mechanisms could explain such an unusual sensitivity of the CheY protein concentration. The first, which is similar to some of the kinetic models in Fig. 10, involves multiple CheY molecules binding to the switch at the flagellar motor. Although not mutually exclusive, either a minimum number of bound CheY molecules are required to affect behavior (threshold), or the switch's affinity for CheY changes for each additional CheY molecule bound (positive cooperativity for binding). A second type of explanation is enzymatic, possibly invoking the zero-order ultrasensitivity phenomenon recently discovered (13, 22). In this phenomenon, high sensitivity can result from varying the substrate saturation of a kinase or phosphatase involved in a cycle of covalent modifications. Since the CheY protein is phosphorylated, the behavioral effect (clockwise rotation) of increasing the CheY concentration could be explained simply by the amplification in the amount of the phosphorylated CheY due to the increased saturation of the kinase. Although a combination of these explanations is very likely, neither explanation can be excluded by the data of this study. For example, kinetic model 10C (Fig. 10), which is consistent with the kinetic data, would be consistent with the second, enzymatic explanation. Clearly, more experiments are required to clarify the mechanism of the motor's switch sensitivity to CheY.

Other molecular switches. The kinetic study of flagellar motors has similarities to studies of gated ion channels, such as the nicotinic acetylcholine receptor. Both systems have two stable modes, with clockwise rotation akin to high ion conductance. Although CheY might have a kinetic role similar to acetylcholine agonists, the biological purpose of such regulation is qualitatively different. The stochastic fluctuations of conduction in ion channels have yet to be assigned a biological function. The stochastic fluctuations of the flagellar motor, however, are necessary to generate the random behavior of wild-type bacteria swimming in a three-dimensional random walk (6, 26). CheY is responsible for some of the stochastic, steady-state behavior of flagellar motors as well as having additional functions in signal transduction.

ACKNOWLEDGMENTS

This work was supported by Public Health Service grant DK09765 from the National Institutes of Health (D.E.K.) and by a predoctoral fellowship from the National Science Foundation (S.C.K.).

ADDENDUM

Interdependence of average rotational intervals. Multistate models could also explain some unusual kinetics observed

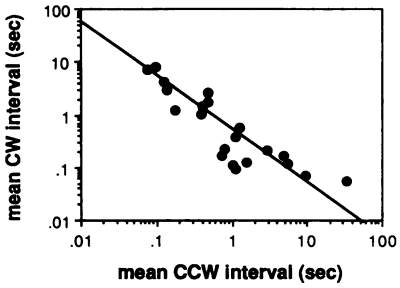

FIG. 11. Interdependence of mean clockwise and mean counterclockwise intervals in individual cells. Cells were the same as those in Fig. 5 and contain CheY in the Δ(*cheA-cheZ*) background. Mean clockwise interval, $<t_{cw}>$, is the average duration of clockwise rotational events. The mean counterclockwise interval is similarly defined. Assuming that $<t_{cw}> \cdot <t_{ccw}> = C$, nonlinear least-squares fitting estimates C to be 0.55 ± 0.03. This curve is included in the figure (solid line).

by Khan and Macnab (17). They altered motor-switching probabilities by perturbing the proton motive force that drives these motors. As motors experience decreasing proton motive force, their angular velocity decreases and they spend more time rotating counterclockwise. Under decreasing proton motive force, the average clockwise interval, $<t_{cw}>$, and the average counterclockwise interval, $<t_{ccw}>$, matched, so that the product of these two quantities appeared to be a constant, 0.5 s^2. In our studies of CheY-induced clockwise rotation in the Δ(*cheA-cheZ*) deletion background, we found that the product of the average interval times also appeared to be a constant, approximately 0.55 s^2, as shown in the log-log plot of Fig. 11. With multistate models such as those proposed in Fig. 10, appropriate rate constants could produce theoretical curves consistent with the observed CheY-induced kinetics. If the transition probabilities between these multiple states were also sensitive to proton motive force, the kinetics observed by Khan and Macnab would be generated. A speculative mechanism would be that proton motive force modulates the motor affinity for CheY, altering the transition rates between kinetic species by altering CheY affinity.

LITERATURE CITED

1. **Anderson, C. R., and C. F. Stevens.** 1973. Voltage clamp analysis of acetylcholine produced end-plate current fluctuations at frog neuromuscular junction. J. Physiol. (London) **235**:655–691.
2. **Bean, R. C., W. C. Sheperd, H. Chan, and J. Eichner.** 1969. Discrete conductance fluctuations in lipid bilayer protein membranes. J. Gen. Physiol. **53**:741–757.
3. **Berg, H. C.** 1974. Dynamic properties of bacterial flagellar motors. Nature (London) **249**:77–79.
4. **Berg, H. C., and S. M. Block.** 1984. A miniature flow cell designed for rapid exchange of media under high-power microscope objectives. J. Gen. Microbiol. **130**:2915–2920.
5. **Berg, H. C., S. M. Block, M. P. Conley, A. R. Nathan, J. N. Power, and A. J. Wolfe.** 1987. Computerized video analysis of tethered bacteria. Rev. Sci. Instrum. **58**:418–423.
6. **Berg, H. C., and D. A. Brown.** 1972. Chemotaxis in *Escherichia coli* analysed by three-dimensional tracking. Nature (London) **239**:500–504.
7. **Blake, M. S., K. H. Johnston, G. J. Russell-Jones, and E. C. Gotschlich.** 1984. A rapid, sensitive method for detection of alkaline phosphatase-conjugated anti-antibody on Western blots. Anal. Biochem. **136**:175–179.
8. **Block, S. M., J. E. Segall, and H. C. Berg.** 1982. Impulse responses in bacterial chemotaxis. Cell **31**:215–226.
9. **Block, S. M., J. E. Segall, and H. C. Berg.** 1983. Adaptation kinetics in bacterial chemotaxis. J. Bacteriol. **154**:312–323.
10. **Clegg, D. O., and D. E. Koshland, Jr.** 1984. The role of a signaling protein in bacterial sensing: behavioral effects of increased gene expression. Proc. Natl. Acad. Sci. USA **81**: 5056–5060.
11. **Colquhoun, D., and F. J. Sigworth.** 1983. Fitting and statistical analysis of single-channel records, p. 191–263. *In* B. Sakmann and E. Neher (ed.), Single-channel recording. Plenum Publishing Corp., New York.
12. **de Boer, H., L. J. Comstock, and M. Vasser.** 1983. The *tac* promoter: functional hybrid derived from the *trp* and *lac* promoters. Proc. Natl. Acad. Sci. USA **80**:21–25.
13. **Goldbeter, A., and D. E. Koshland, Jr.** 1981. An amplified sensitivity arising from covalent modification in biological systems. Proc. Natl. Acad. Sci. USA **78**:6840–6844.
14. **Hess, J. F., R. B. Bourret, and M. I. Simon.** 1988. Histidine phosphorylation and phosphoryl group transfer in bacterial chemotaxis. Nature (London) **336**:139–143.
15. **Hess, J. F., K. Oosawa, N. Kaplan, and M. I. Simon.** 1988. Phosphorylation of three proteins in the signaling pathway of bacterial chemotaxis. Cell **53**:79–87.
16. **Hess, J. F., K. Oosawa, P. Matsumura, and M. I. Simon.** 1987. Protein phosphorylation is involved in bacterial chemotaxis. Proc. Natl. Acad. Sci. USA **84**:7609–7613.
17. **Khan, S., and R. M. Macnab.** 1980. The steady-state counterclockwise/clockwise ratio of bacterial flagellar motors is regulated by protonmotive force. J. Mol. Biol. **138**:563–597.
18. **Khan, S., R. M. Macnab, A. L. DeFranco, and D. E. Koshland, Jr.** 1978. Inversion of a behavioral response in bacterial chemotaxis: explanation at the molecular level. Proc. Natl. Acad. Sci. USA **75**:4150–4154.
19. **Kobayashi, S., K. Maeda, and Y. Imae.** 1977. Apparatus for detecting rate and direction of rotation of tethered bacterial cells. Rev. Sci. Instrum. **48**:407–410.
20. **Kuo, S. C., and D. E. Koshland, Jr.** 1987. Roles of *cheY* and *cheZ* gene products in controlling flagellar rotation in bacterial chemotaxis of *Escherichia coli*. J. Bacteriol. **169**:1307–1314.
21. **Lapidus, I. R., M. Welch, and M. Eisenbach.** 1988. Pausing of flagellar rotation is a component of bacterial motility and chemotaxis. J. Bacteriol. **170**:3627–3631.
22. **LaPorte, D. E., and D. E. Koshland, Jr.** 1983. Phosphorylation of isocitrate dehydrogenase as a demonstration of enhanced sensitivity in covalent regulation. Nature (London) **305**:286–290.
23. **Larsen, S. H., J. Adler, J. J. Gargus, and R. W. Hogg.** 1974. Chemomechanical coupling without ATP: the source of energy for motility and chemotaxis in bacteria. Proc. Natl. Acad. Sci. USA **71**:1239–1243.
24. **Larsen, S. H., R. W. Reader, E. N. Kort, W.-W. Tso, and J. Adler.** 1974. Change in direction of flagellar rotation is the basis of the chemotactic response in *Escherichia coli*. Nature (London) **249**:74–77.
25. **Macnab, R. M.** 1986. Proton driven bacterial flagellar motor. Methods Enzymol. **125**:563–581.
26. **Macnab, R. M., and D. E. Koshland, Jr.** 1972. Gradient sensing mechanism in bacterial chemotaxis. Proc. Natl. Acad. Sci. USA **69**:2509–2512.
27. **Macnab, R. M., and D. E. Koshland, Jr.** 1974. Bacterial motility and chemotaxis: light-induced tumbling response and visualization of individual flagella. J. Mol. Biol. **84**:399–406.
28. **Maniatis, T., E. F. Fritsch, and J. Sambrook.** 1982. Molecular cloning: a laboratory manual. Cold Spring Harbor Laboratory, Cold Spring Harbor, N.Y.
29. **Matsumura, P., J. J. Rydel, R. Linzmeier, and D. Vacante.** 1984. Overexpression and sequence of the *Escherichia coli cheY* gene and biochemical activities of the CheY protein. J. Bacteriol. **160**:36–41.
30. **Neher, E., and B. Sakmann.** 1976. Single-channel currents recorded from membrane of denervated frog muscle fibres. Nature (London) **260**:799–801.
31. **Ninfa, A. J., E. G. Ninfa, A. N. Lupas, A. Stock, B. Magasanik, and J. Stock.** 1988. Crosstalk between bacterial chemotaxis

signal transduction proteins and regulators of transcription of the Ntr regulon: evidence that nitrogen assimilation and chemotaxis are controlled by a common phosphotransfer mechanism. Proc. Natl. Acad. Sci. USA **85**:5492–5496.
32. **Parkinson, J. S., and S. E. Houts.** 1982. Isolation and behavior of *Escherichia coli* deletion mutants lacking chemotaxis functions. J. Bacteriol. **151**:106–113.
33. **Parkinson, J. S., and S. R. Parker.** 1979. Interaction of the *cheC* and *cheZ* gene products is required for chemotactic behavior in *Escherichia coli*. Proc. Natl. Acad. Sci. USA **76**:2390–2394.
34. **Parkinson, J. S., S. R. Parker, P. B. Talbert, and S. E. Houts.** 1983. Interactions between chemotaxis genes and flagellar genes in *Escherichia coli*. J. Bacteriol. **155**:265–274.
35. **Ravid, S., P. Matsumura, and M. Eisenbach.** 1986. Restoration of flagellar clockwise rotation in bacterial envelopes by insertion of the chemotaxis protein CheY. Proc. Natl. Acad. Sci. USA **83**:7157–7161.
36. **Rubik, B. A., and D. E. Koshland, Jr.** 1978. Potentiation, desensitization, and inversion of response in bacterial sensing of chemical stimuli. Proc. Natl. Acad. Sci. USA **75**:2820–2824.
37. **Silverman, M., and M. Simon.** 1974. Flagellar rotation and the mechanism of bacterial motility. Nature (London) **249**:73–74.
38. **Simons, R. W., F. Houman, and N. Kleckner.** 1987. Improved single and multicopy *lac*-based cloning vectors for protein and operon fusions. Gene **53**:85–96.
39. **Smith, J. M., E. H. Rowsell, J. Shioi, and B. L. Taylor.** 1988. Identification of a site of ATP requirement for signal processing in bacterial chemotaxis. Proc. Natl. Acad. Sci. USA **83**:8987–8991.
40. **Stock, A., D. E. Koshland, Jr., and J. Stock.** 1985. Homologies between the *Salmonella typhimurium* CheY protein and proteins involved in the regulation of chemotaxis, membrane protein synthesis, and sporulation. Proc. Natl. Acad. Sci. USA **82**:7989–7993.
41. **Stock, A. M., and J. B. Stock.** 1987. Purification and characterization of the CheZ protein of bacterial chemotaxis. J. Bacteriol. **169**:3301–3311.
42. **Takeuchi, A., and N. Takeuchi.** 1959. Active phase of frog's end plate potential. J. Neurophysiol. **22**:395–411.
43. **Towbin, H., T. Staehelin, and J. Gordon.** 1979. Electrophoretic transfer of proteins from polyacrylamide gels to nitrocellulose sheets: procedure and some applications. Proc. Natl. Acad. Sci. USA **76**:4350–4354.
44. **Vogel, H. J., and D. M. Bonner.** 1956. Acetylornithinase of *Escherichia coli*: partial purification and some properties. J. Biol. Chem. **218**:97–106.
45. **Wolfe, A. J., M. P. Conley, T. J. Kramer, and H. C. Berg.** 1987. Reconstitution of signaling in bacterial chemotaxis. J. Bacteriol. **169**:1878–1885.
46. **Wylie, D., A. M. Stock, C.-Y. Wong, and J. B. Stock.** 1988. Sensory transduction in bacterial chemotaxis involves phosphotransfer between Che proteins. Biochem. Biophys. Res. Commun. **151**:891–896.
47. **Yamaguchi, S., S.-I. Aizawa, M. Kihara, J. Isomura, C. J. Jones, and R. M. Macnab.** 1986. Genetic evidence for a switching and energy-transducing complex in the flagellar motor of *Salmonella typhimurium*. J. Bacteriol. **168**:1172–1179.
48. **Yamaguchi, S., H. Fujita, A. Ishihara, S.-I. Aizawa, and R. M. Macnab.** 1986. Subdivision of multifunctional flagellar genes of *Salmonella typhimurium* into regions responsible for assembly, rotation, and switching. J. Bacteriol. **166**:187–193.